Phonon Spectra and Thermal Properties of Some fcc Metals Using the Embedded-Atom Method

Q. Bian[†],[*] S.K. Bose, and R.C. Shukla
Department of Physics, Brock University, St. Catharines, Ontario L2S 3A1, Canada
(Dated: February 3, 2008)

By employing the analytic embedded-atom potentials of Mei *et al.* [Phys. Rev. B 43, 4653 (1991)] we have calculated the phonon dispersion spectra for six fcc metals: Cu, Ag, Au, Ni, Pd and Pt. We have also investigated thermal properties of these metals within the quasiharmonic approximation. Results for the lattice constants, coefficients of linear thermal expansion, isothermal and adiabatic bulk moduli, heat capacities at constant volume and constant pressure, Debye temperatures and Grüneisen parameters as a function of temperature are presented. The computed results are compared with the available experimental data. The comparison shows a generally good agreement between the calculated and experimental values for all thermodynamic properties studied. Isothermal and adiabatic bulk moduli and the specific heats are reproduced reasonably well, while the Grüneisen parameter and Debye temperature are underestimated by about 10%. The calculated phonon frequencies for Ag and Cu agree well with the results from inelastic neutron scattering experiments. However, there is considerable room for improvement in the phonon frequencies for Ni, Pd, Pt and Au, particularly at high phonon wave vectors close to the Brillouin zone boundary. The coefficient of linear thermal expansion is underestimated in most cases except for Pt and Au. The results are good for Pt up to 1000K and for Au up to 500 K.

PACS numbers: 63.20.-e, 65.40.-b

I. INTRODUCTION

The inadequacy of pure pair-potential models to describe metallic cohesion is well-known and has been adequately documented.[1,2] Various approaches, at varying levels of sophistication, have been used to address the volume-dependence of the energy of a metallic system originating from the presence of the interacting electron gas. These range from using volume-dependent parameters in the pair potential itself[3] to writing the total energy as a sum of pair potentials plus an empirical volume/density-dependent term[4,5,6,7,8] or an electronic band(bond) energy term.[9,10] The latter is often written in terms of the first few moments of the electronic density of states in the tight-binding approximation.[11,12] For transition metals, invoking a simplified model of rectangular *d*-density of states due to Friedel,[13] the bond energy term is sometimes approximated simply via the second moment of the density of states.[14,15,16,17]

An approach that has been widely used in this context is the embedded atom method (EAM) of Daw and Baskes,[18,19] where the energy of the metal is viewed as the energy to embed an atom into the local electron density provided by the remaining atoms of the system, plus a sum of pair interaction potentials between the atoms. This method, which was developed almost simultaneously by Finnis and Sinclair,[4] starts with the ansatz:

$$E_{tot} = \sum_i F_i(\rho_{h,i}) + \frac{1}{2}\sum_{\substack{i,j \\ (i\neq j)}} \Phi(R_{ij}), \qquad (1)$$

$$\rho_{h,i} = \sum_{j(j\neq i)} f_j(R_{ij}), \qquad (2)$$

where E_{tot} is the total internal energy, $\rho_{h,i}$ is the host electron density at atom i due to all other atoms, f_j is the electron density of atom j as a function of distance from its center, R_{ij} is the separation distance between atoms i and j. The function $F_i(\rho_{h,i})$, called the embedding energy, is the energy to embed atom i in an electron density $\rho_{h,i}$. Φ_{ij} is a two-body central pair potential between atoms i and j. The host electron density $\rho_{h,i}$ is assumed to be a linear superposition of spherically symmetric contributions from all individual atoms except atom i.

In the model proposed by Finnis and Sinclair[4] the total energy of a system of atoms is assumed to consist of a binding term proportional to the square-root of the local density and a repulsive pairwise potential term. Another approach to this type of theory was provided by Manninen,[20] Jacobsen, Nϕrskov, and Puska,[21] who derived the functional form of the two terms in Eq.(1) by using the density functional theory. Although Daw and Baskes[18,19] had also used the density functional theory to justify the use of Eq.(1), in most applications of the method the two terms of Eq.(1) were written in terms of parameters that were fitted to observed properties of the system. In this sense, the EAM remains an empirical or at best a semi-empirical method. However, the simplicity and ease with which it could be applied to a large variety of situations has led to its wide use in the study of liquids,[22,23,24] alloys,[25,26] surfaces and interfaces,[27,28,29,30,31,32,33,34,35,36] impurities and other defects in solids.[18,19,37] Relevant to the present work is the study by Foiles and Adams,[38] who investigated some thermodynamic properties of six fcc metals: Cu, Ag, Au, Ni, Pd and Pt via quasiharmonic calculations and molecular dynamics simulation using the EAM

potentials developed by Foiles, Baskes and Daw.[25]

By replacing the atomic electron density with an exponentially decaying function, Johnson[34] developed a set of analytic EAM functions for the nearest neighbor model of fcc metals. However, this model had the limitation that all materials were forced to have the same anisotropy ratio of the shear moduli : $c_{44}/(c_{11}-c_{12})=1$. Oh and Johnson[39] extended the model beyond nearest neighours, at the cost of sacrificing the simple analytic form. Mei *et al.*[40] have overcome this challenge and extended this nearest-neighbor model into the one in which the embedded atom potentials are analytic and valid for any choice of the cut-off distance. In particular they derived the values of the parameter for their EAM potential and density functions for six fcc metals: Ni, Pd, Pt, Cu, Ag, and Au. They used this EAM potential in a molecular dynamics study of thermal expansion and specific heat of liquid Cu as a function of temperature, using a cut-off for the potential and embedding functions somewhere between the third and fourth neighbors for the corresponding crystalline case. In later studies they applied the model to study self-diffusion in the liquid phase of the above six metals[23] and the melting in Al.[24] Kuiying *et al.*[41] have used this EAM potential in a molecular dynamics study of the local structure in supercooled liquid and solid Cu and Al. Although Mei *et al.*[40] had derived the values of the EAM parameters for six fcc metals: Ni, Pd, Pt, Cu, Ag, and Au, to this date a systematic study of the vibrational and thermodynamic properties of these solids in the bulk crystalline phase using these parameters has not been carried out. This work presents such a study for the first time and explores to what extent this particular EAM model is successful in reproducing the experimentally observed phonon spectra and thermodynamic properties for the above six bulk fcc metals.

The organization of this paper is as follows: in section II we discuss some details of the EAM potentials of Mei *et al.*[40] and its implementation in the present work. In section III we discuss the calculated phonon spectra for the six fcc metals and their agreement with the experimental results. In section IV we discuss the calculated and the corresponding experimental values of various properties: thermal expansion coefficients, isothermal and adiabatic bulk moduli, specific heats at constant volumes and pressures, the Debye temperature and the Grüneisen parameter as a function of temperature. In section V we summarize our results and conclusions about the validity of this particular EAM model.

II. THE MODEL

The embedding function $F(\rho)$ and the two-body potential $\Phi(R)$ in Eq. (1) of Mei *et al.* are given by:

$$\begin{aligned} F(\rho) &= -E_c\left[1-\frac{\alpha}{\beta}\ln\left[\frac{\rho}{\rho_e}\right]\right]\left[\frac{\rho}{\rho_e}\right]^{\alpha/\beta} \\ &+ \frac{1}{2}\phi_e\sum_{\Lambda} s_\Lambda \exp[-(p_\Lambda-1)\gamma] \\ &\times\left[1+(p_\Lambda-1)\delta - p_\Lambda\frac{\delta}{\beta}\ln\left[\frac{\rho}{\rho_e}\right]\right] \\ &\times\left[\frac{\rho}{\rho_e}\right]^{p_\Lambda\frac{\gamma}{\beta}}, \end{aligned} \tag{3}$$

$$\Phi(R) = -\phi_e[1+\delta(R/R_{1e}-1)]\exp[-\gamma(R/R_{1e}-1)], \tag{4}$$

with

$$\rho = \sum_{\Lambda} s_\Lambda f(R_\Lambda), \tag{5}$$

$$f(R) = f_e\sum_{\tau=0}^{\kappa} c_\tau (R_{1e}/R)^\tau. \tag{6}$$

In Eq. (3), α is defined by

$$\alpha = (9B_e\Omega_e/E_c)^{1/2}, \tag{7}$$

Ω is the atomic volume, B the bulk modulus, E_c the cohesive energy. The subscript e refers to the equilibrium value. s_Λ in Eq. (5) is the number of atoms on the Λ-th neighbor shell with respect to a given reference atom. p_Λ refers to the Λ-th neighbor shell via

$$R_\Lambda = p_\Lambda R_1, \Lambda = 1, 2, ..., \tag{8}$$

where R_1 is the distance of the first neighbor shell with respect to a reference atom and R_Λ the distance of the Λth-neighbor shell. The constants p_Λ depend on the crystal structure type: for the fcc structure $p_\Lambda = \sqrt{\Lambda}$.

Mei *et al.*[40] used $\kappa = 5$ in Eq.(6) to fit the atomic charge density ρ. Only ratios of electronic densities appear in Eq.(3) and hence ρ_e cancels out. The constant f_e was set equal to $\rho_e/12$. The constant β was taken from previous works by Johnson.[26,34] The remaining constants were obtained by fitting to the measured values of unrelaxed vacancy formation energy and the elastic constants, all of which were calculated by using three shells of neighbors for all the fcc metals considered. The exact details of the fitting procedure used is given in Ref. [40].

The values of the constants thus generated and given in Table I of Mei *et al.*,[40] were used in the present work with one notable difference. Mei *et al.*[40] obtained the values of the parameters in their model by considering three shells of neighbors for the fcc solid. In the molecular dynamics study of liquid and solid Cu, they used a cut-off

distance in their embedding function and pair-potential lying between the third and the fourth nearest neighbors. We have calculated the elastic constants C_{11}, C_{12} and C_{44} using the homogeneous deformation method and also from the long wavelength phonons and studied their variation with respect to the number of neighbor shells included in the calculation. For three shells of neighbors our results obtained via the homogeneous deformation method agrees well with those obtained by Mei *et al.*.[40] However, the values obtained via the homogeneous deformation method and from long wavelength phonons differ significantly from each other as well as from the experimental values. The differences in the results obtained by the two methods as well as between the calculated and experimental values, decrease on increasing the number of neighbor shells in the calculation and practically disappear as the number of neighbor shells reaches six. Based on this result, we have calculated the phonon spectra and all the physical properties by using six shells of neighbors for this model of EAM. We have compared the phonon frequencies for the test case of Cu by using three to six shells of neighbors The maximum difference, which is found for low energy phonons, between the three and six neighbor shells is of the order of 1%. The differences in the phonon frequencies between the three and six neighbor shell calculations decrease with increasing wave vector, and at the zone boundary they are of the order of .01%. The static energy of the solid, given by Eq.(1), changes by $\sim 0.7\%$ as the number of shells increases from three to six. However, there is virtually no change in the location of the minimum in the static energy as a function of lattice parameter, as well as the curvature at the location of the minimum.

III. PHONONS

The phonon spectra were calculated as usual by diagonalizing the dynamical matrix, obtained from the Fourier transform of the force constant tensor $\mathbf{\Phi}_{ij}(l,m)$ given by

$$\mathbf{\Phi}_{ij}(l,m) = \frac{\partial^2 E_{tot}}{\partial R^i(l)\partial R^j(m)}, \qquad (9)$$

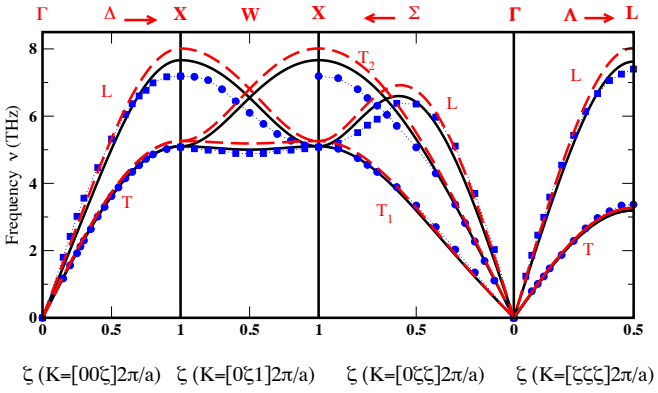

FIG. 1: Phonon dispersion curves for Cu. The solid lines are the calculated phonon dispersion curves at the room temperature equilibrium lattice parameter of 3.6131 Å.[42] The square and round points are the experimental data at 296K from Ref. [43]. L and T represent transverse and longitudinal modes, respectively.

where l, m are the labels of the atoms. For E_{tot} given by Eqs.(1) and (2), and with $l \neq m$

$$\begin{aligned}
\mathbf{\Phi}_{ij}(l,m) \;=\; & -F_l'(\rho_l) f_m''(R_{lm}) \frac{R_{lm}^j R_{lm}^i}{R_{lm}^2} \\
& -F_m'(\rho_m) f_l''(R_{lm}) \frac{R_{lm}^j R_{lm}^i}{R_{lm}^2} \\
& -\Phi''(R_{lm}) \frac{R_{lm}^j R_{lm}^i}{R_{lm}^2} - [F_l'(\rho_l) f_m'(R_{lm}) \\
& +F_m'(\rho_m) f_l'(R_{lm}) + \Phi'(R_{lm})] \\
& \times \left\{ \frac{\delta_{ij}}{R_{lm}} - \frac{R_{lm}^i R_{lm}^j}{R_{lm}^3} \right\} + \sum_{n(\neq l,m)} F_n''(\rho_n) \\
& \times f_l'(R_{ln}) f_m'(R_{mn}) \frac{R_{mn}^j}{R_{mn}} \frac{R_{ln}^i}{R_{ln}}, \qquad (10)
\end{aligned}$$

where the prime in the function in the above equation denotes the derivative of the function with respect to its argument. Though written somewhat differently the above expression is in agreement with that derived by Finnis and Sinclair.[4]

The calculated phonon frequencies for the six fcc metals Ni, Pd, Pt and Cu, Ag, Au are plotted in Figs.(1-6). In Fig. (1) we compare the calculated phonon spectrum in Cu with the experimental results of Svensson, Brockhouse and Rowe.[43] The squares and the circles represent the phonon frequencies from the inelastic neutron scattering experiment at room temperature (296 K), while the solid line denotes the calculated spectrum. For estimating the importance of the embedding term we have used dashed lines to show the frequencies obtained by considering only the pair potential term, i.e., neglecting the contribution from the embedding function. The

pair potential and the embedding terms contribute to the force constant with opposite signs: without the embedding term the phonon frequencies at high values of the wave vectors would have much worse agreement with the measured frequencies. We find that the three-body terms coming from the embedding function (the last term in Eq.(10)) have a negligible effect on the phonon frequencies, the values obtained with and without these terms are virtually indistinguishable. We have also compared the calculated phonon frequencies with the experimental values for off-symmetry wave vectors, as given by Nilsson and Ronaldson.[44] The agreement is similar to that for the wave vectors along the symmetry directions, in the sense that the agreement is very good for small wave vectors, while becoming progressively worse with increasing wave vectors to the same extent as for the symmetry direction wave vectors shown in Fig. (1).

The term involving the embedding function in Eq.(1) contributes about $\frac{1}{4}$ to $\frac{1}{3}$ of the total energy for the model of Mei *et al.*,[40] but their contribution to vibrational frequencies is less than 10%. Hence, the embedding term contributes to the temperature variation of thermodynamic properties mainly via the static part of the free energy.

For Cu the phonon frequencies calculated by considering only the contributions from the nearest neighbors in the fcc structure produce about 90% of the final converged frequencies originating from all neighbors. This is in agreement with the observation of Svensson *et al.*,[43] who used several Born-von Kármán force constant models involving neighbors up to various different shells to study the agreement between the calculated phonon frequencies and those from the inelastic neutron scattering experiment. Their least square fits of atomic and planar force constants to the observed phonon frequencies indicate that the nearest neighbor forces dominate in Cu, although longer range forces extending at least to the sixth-nearest neighbors are needed for a complete agreement between the calculated and experimental frequencies. A similar result was found by Nilsson and Ronaldson[44] in a neutron crystal spectrometer study of phonon frequencies in Cu at wave vectors of both symmetry and off-symmetry points in the Brillouin zone at a temperature of 80 K.

Among the six fcc metals, the agreement between the calculated and experimental phonon spectra is almost perfect for Ag and only slightly less so for Cu. For all other metals the agreement becomes increasingly worse with increasing wave vectors in all the symmetry directions, the worst case being that of Au. For Pd, Pt and Au the calculated phonon frequencies are underestimated with respect to the experimental results, while they are somewhat overestimated for Ni. For Cu,[28] Ag,[29] Ni and Pd,[27] this trend as well as the level of agreement between the calculated and experimental phonon frequencies is the same as in the EAM scheme of Daw and Baskes,[19] where the total charge density at an atomic location is calculated from the *ab initio* Hartree-Fock results for free

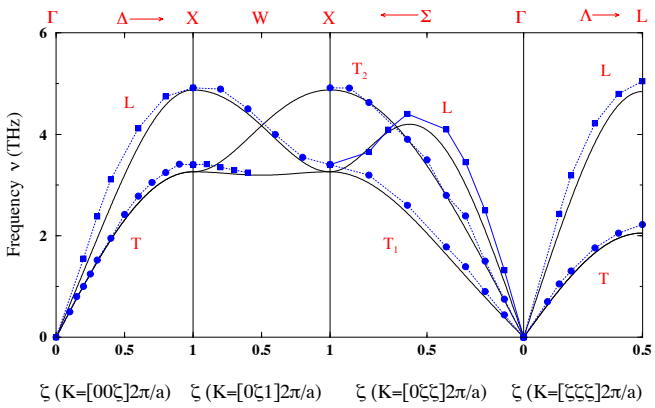

FIG. 2: Phonon dispersion curves for Ag. The solid lines are the calculated phonon dispersion curves at the room temperature equilibrium lattice parameter.[42] The square and round points are the experimental data from Ref.[50] at room temperature. L and T represent transverse modes and longitudinal modes respectively.

atom charge densities.[45,46] As pointed out by Daw and Hatcher,[27] as long as the fitting is done primarily to elastic constants, which involve phonons near the zone center only, the agreement for high frequency phonons near the zone boundary is not guaranteed. In this respect, phonons calculated via *ab initio* electronic structure methods, which can capture the details of Fermi surface topology without resorting to any empirical fitting procedure, can yield superior results,[47,48] although results do vary depending on the method of electronic structure calculation and details of the implementation of exchange-correlation potentials, etc.[49] Of course if one is simply interested in the phonon spectra, Born-von Kármán fit to force constants can yield very satisfactory results.[43] Note that the agreement with the experimental phonon spectra for Cu obtained by Cowley and Shukla[3] by using a nearest neighbor Born-Mayer potential with volume-dependent prefactor is as good as obtained in the present EAM model. The total energy of the crystal in this study by Cowley and Shukla[3] consisted of kinetic, exchange and correlation energies of the electron gas and an electron-ion interaction term in addition to the nearest neighbor Born-Mayer potential.

IV. THERMODYNAMIC PROPERTIES

In the quasiharmonic approximation, the total Helmholtz free energy of the crystal at temperature T and volume V or lattice constant a is given by

$$\begin{aligned} F(a,T) &= E_{tot}(a) + F_{vib}(a,T) \\ &= E_{tot}(a) + k_B \sum_{\mathbf{K}s} \\ &\quad \times \ln\{2sinh\frac{\hbar\omega_s(\mathbf{K},a)}{2k_BT}\} \end{aligned} \tag{11}$$

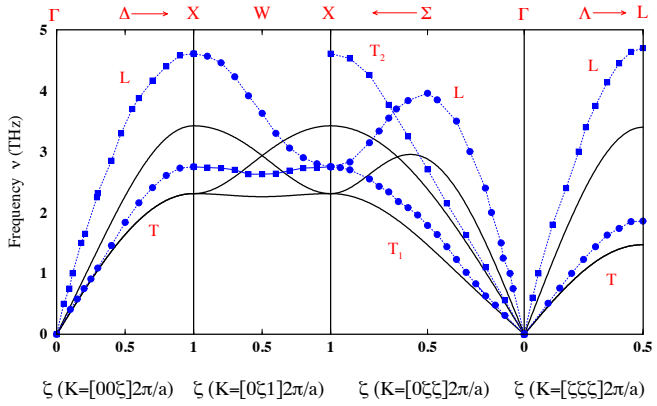

FIG. 3: Phonon dispersion curves for Au. The solid lines, square and round points and the symbols L and T have the same meanings as in Figs. 1 and 2. The experimental data at 296K is from Ref. [51]

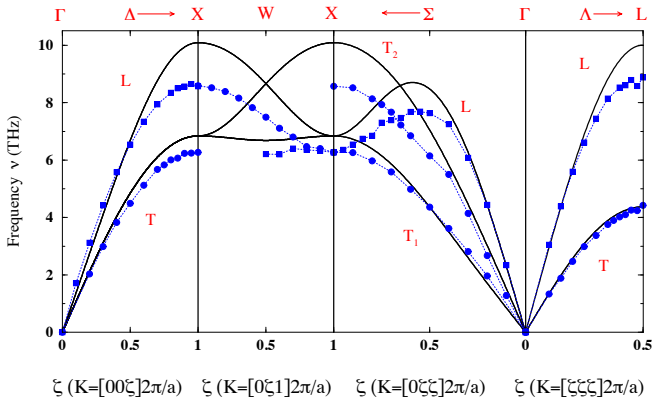

FIG. 4: Phonon dispersion curves for Ni. The solid lines, square and round points and the symbols L and T have the same meanings as in Figs. 1 and 2. The experimental data taken at 296K is from Ref.[52].

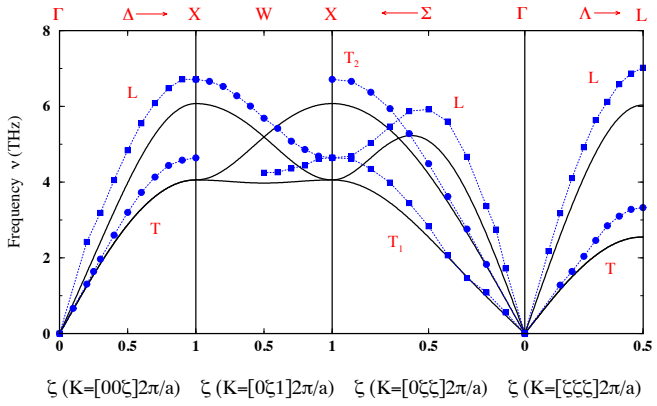

FIG. 5: Phonon dispersion curves for Pd. The solid lines, square and round points and the symbols L and T have the same meanings as in Figs. 1 and 2. The experimental data taken at 120K is from Ref. [53].

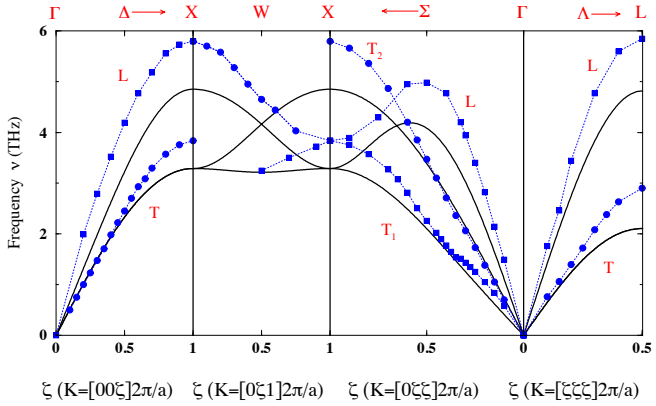

FIG. 6: Phonon dispersion curves for Pt. The solid lines, square and round points and the symbols L and T have the same meanings as in Figs. 1 and 2. The experimental data is from Ref.[54].

where E_{tot} is the static total energy given by Eq.(1) at a given volume V or lattice constant a. $\omega_s(\mathbf{K}, a)$ is the frequency of sth mode for a given wave vector $\mathbf{K}$ and lattice constant a. $\hbar$ and K_B are the Planck's and Boltzmann's constants, respectively.

All thermodynamic properties are calculated from the free energy given by Eq.(11). In obtaining the wave vector sum in Eq.(11) we consider a 20^3 uniform grid in the Brillouin zone (BZ) giving 256 wave vectors in the irreducible part. The sum is performed using these 256 wave vectors, appropriately weighted according to the point-group symmetry of the fcc solid. Temperature variation of thermodynamic properties is studied from $0K$ to $1400K$ in steps of $2K$.

At a given temperature T, the equilibrium lattice parameter is determined by the minmum of the Helmholtz free energy, i.e.,

$$\left(\frac{\partial F(a,T)}{\partial a}\right)_T = \frac{\partial E_{tot}(a)}{\partial a} + \left(\frac{\partial F_{vib}(a,T)}{\partial a}\right)_T = 0. \quad (12)$$

The variation of lattice constant with temperature for the six fcc metals is shown in Fig.(7). It should be noted that our quasiharmonic results for Cu agree very well with those obtained by Mei *et al.*[40] using molecular dynamics simulation. A small difference, increasing with temperaure, appears above 900 K due to the anaharmonic effects not included in the quasiharmonic approach. The results for all the six metals are as good as those obtained by Foiles and Admas[38] using the EAM potentials of Foiles, Baskes and Daw[25]

The coefficient of linear thermal expansion is given by

$$\alpha(T) = \frac{1}{a_e(T)}\left(\frac{da_e(T)}{dT}\right)_p. \quad (13)$$

In experimental works Eq.(13) is often replaced with[55,56]

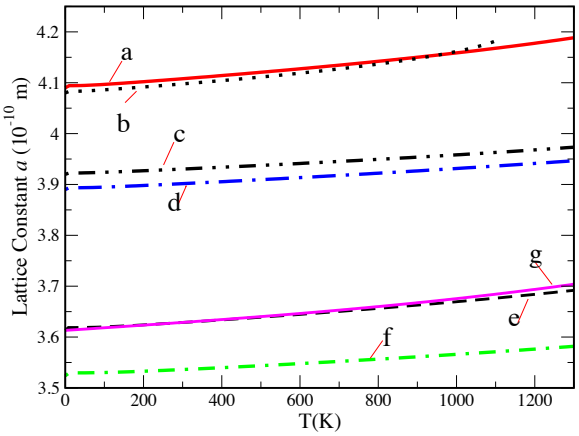

FIG. 7: Lattice Constant Against Temperature for the fcc Metals. Line a is for Ag, b is for Au, c is for Pt, d is for Pd, e is for Cu, and f is for Ni. Line g denotes the results of the MD simulation Mei *et al.* [40] for Cu.

$$\alpha(T) = \frac{1}{a_e(T_c)}\left(\frac{da_e(T)}{dT}\right)_p, \tag{14}$$

where T_c is a reference temperature, usually taken to be the room temperature. To be consistent with experimental and other theoretical work,[55] we take $T_c = 293$. Using Eq. (14), we calculate the coefficients of linear expansion $\alpha(T)$ for the six fcc metals and plot them in Figs.(9 - 10) along with the experimental values. Thermal expansion coefficients for Cu, Ag and Ni calculated by Shukla and MacDonald[56] and MacDonald and MacDonald[55] based on empirical nearest neighbor central force model and incorporating two lowest order, cubic and quartic, anharmonic effects show much better agreement with experiment than those given by the present EAM model in the quasiharmonic approximation.

The isothermal bulk modulus at a temperature T is given by

$$B(T) = -V\left(\frac{\partial P}{\partial V}\right)_T, \; P = -\frac{\partial F}{\partial V}. \tag{15}$$

or

$$\begin{aligned} B(T) &= V\left(\frac{\partial^2 F}{\partial V^2}\right)_T \\ &= V\left(\frac{\partial^2 E_{tot}}{\partial V^2}\right) + V\left(\frac{\partial^2 F_{vib}(a,T)}{\partial V^2}\right)_T. \end{aligned} \tag{16}$$

The second derivatives in Eq.(16) are obtained via numerical differentiation and the results are compared with the available experimental data in Figs. (14 - 15). Both the values and the trend, a small decrease with increasing temperature, are reproduced reasonably well in the calculation.

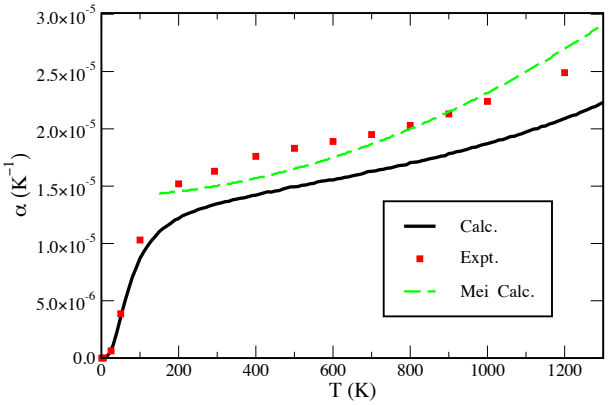

FIG. 8: Coefficient of linear thermal expansion $\alpha(T)$ as a function of temperature for Cu. the solid line is the calculated values, the square points are the experimental values from Ref. [57], and the dashed line is the results of the MD simulation of Mei *et al.* [40]

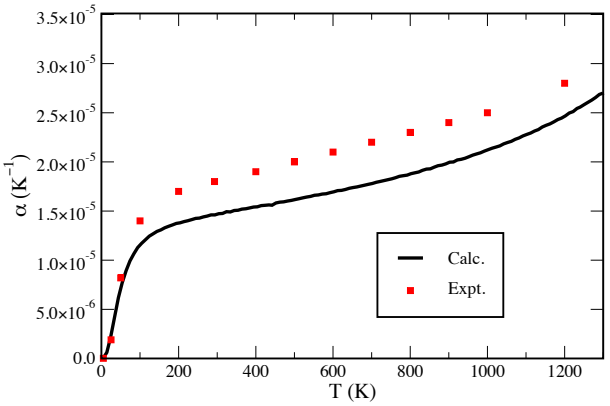

FIG. 9: Coefficient of linear thermal expansion $\alpha(T)$ as a function of temperature for Ag. The solid line denotes the calculated values, and the square points represent the experimental values from Ref. [57].

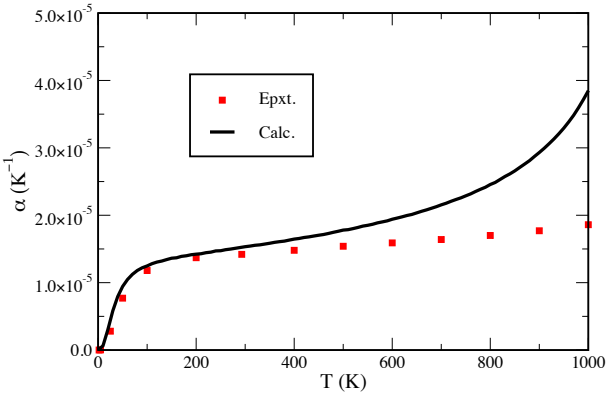

FIG. 10: Coefficient of linear thermal expansion $\alpha(T)$ as a function of temperature for Au. The solid line denotes the calculated values, and the square points represent the experimental values from Ref. [57].

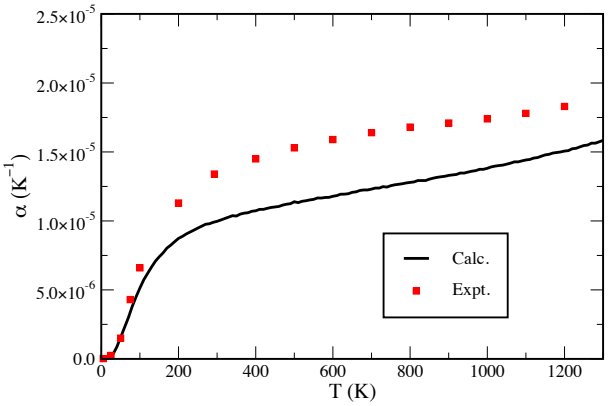

FIG. 11: Coefficient of linear thermal expansion $\alpha(T)$ as a function of temperature for Ni. The solid line denotes the calculated values, and the square points represent the experimental values from Ref. [57].

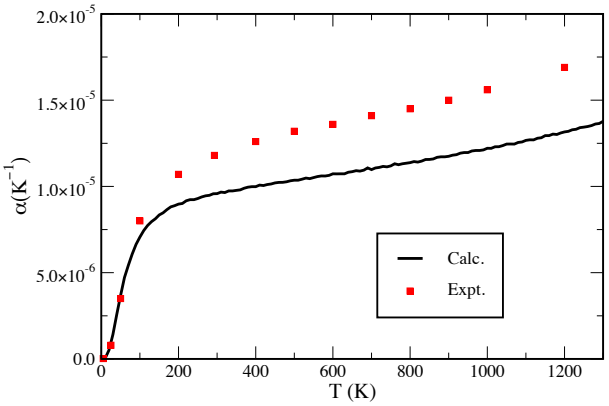

FIG. 12: Coefficient of linear thermal expansion $\alpha(T)$ as a function of temperature for Pd. The solid line denotes the calculated values, and the square points represent the experimental values from Ref. [57].

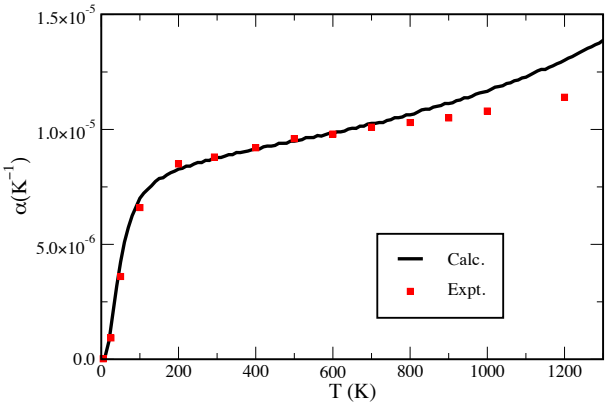

FIG. 13: Coefficient of linear thermal expansion $\alpha(T)$ as a function of temperature for Pt. The solid line denotes the calculated values, and the square points represent the experimental values from Ref. [57].

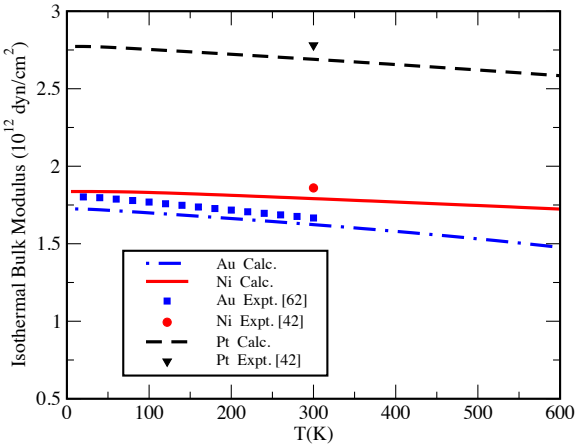

FIG. 14: Isothermal bulk modulus $B(T)$ as a function of temperature for Au, Ni and Pt.

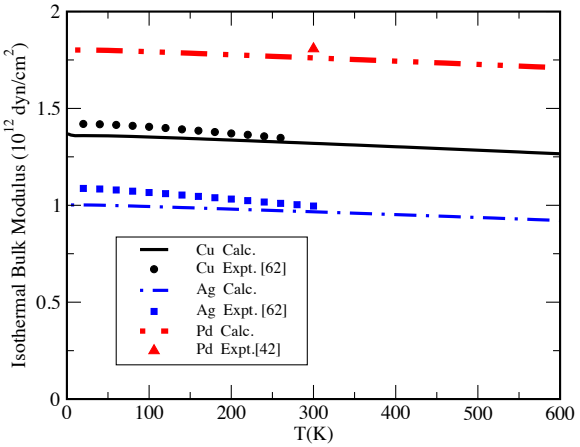

FIG. 15: Isothermal bulk modulus $B(T)$ as a function of temperature for Ag, Cu and Pd.

The specific heat at constant volume C_V can be obtained from the temperature derivative of the total energy. However, the contribution from the electrons excited across the Fermi level cannot be obtained from the EAM expression. Hence we write the specific heat at constant volume as

$$C_V(T) = C_V^{ph}(T) + C_V^{el}(T). \tag{17}$$

where the phonon part is obtained from the EAM model via

$$\begin{aligned} C_V^{ph}(T) &= \sum_{\mathbf{K},s} C_V(\mathbf{K}s) \\ &= k_B \sum_{\mathbf{K}s} \left\{ \frac{\hbar\omega_s(\mathbf{K})}{2k_BT} \right\}^2 \\ &\quad \times \frac{1}{sinh^2[\hbar\omega_s(\mathbf{K})/2k_BT]}. \end{aligned} \tag{18}$$

We estimate the electronic part $C_V^{el}(T)$ via the well-

known expression:

$$C_V^{el}(T) = \frac{\pi^2}{3} k_B^2 N(E_F) T \qquad (19)$$

where $N(E_F)$ is the electronic density of states at the Fermi level E_F. In the above expressions we consider the specific heats and $N(E_F)$ to be per atom. We use the well-known and well-documented Stuttgart TB-LMTO (Tight Binding Linear Muffin-tin Orbitals) code[58] to compute the values of $N(E_F)$ for various lattice parameters. Our results agree well with those given by other methods.[59] With increasing temperature, lattice parameter increases and electronic bands become narrower, resulting in a slight increase in $N(E_F)$. However, this increase is negligible and the variation of $C_V^{el}(T)$ with temperature remains essentially linear. We have actually calculated the $N(E_F)$ for 5-6 values of lattice parameters in the entire temperature range and used linear interpolation to find the values at all other lattice parameters. Eq.(19), which is based on the independent fermionic quasiparticle picture,[60,61] includes all the electron-ion, exchange and correlation effects as incorporated within the framework of density functional theory. What is neglected is the electron-phonon interaction,[60,61] which is presumably small for most of the metals considered, as none of these exhibits superconductivity down to almost absolute zero of temperature. Theoretical calculations[47] of electron-phonon interaction show that for Cu it is indeed negligible, while for Pd it may not be so. Since the values of the electron-phonon coupling constant are known only for a few of these metals, we have simply ignored this contribution. The experimental values contain the effects of electron-phonon interaction in addition to the contributions from vacancies[55] and other defects. Note that in the high temperature limit the calculated quasiharmonic value of $C_V^{ph}(T)$ reaches the classical harmonic value $3K_B$ per atom, as it should.

We calculate the specific heat at constant pressure C_P by using the relation:

$$C_P(T) - C_V(T) = -T\left(\frac{\partial V}{\partial T}\right)_P^2 \left(\frac{\partial P}{\partial V}\right)_T. \qquad (20)$$

or

$$C_P(T) = C_V^{ph}(T) + C_V^{el}(T) + \frac{9}{4}\alpha^2(T) B(T) a_e^3(T) T. \qquad (21)$$

Figs.(16 - 21) show the temperature-dependence of heat capacity at constant volume C_V^{ph}, at constant pressure C_P and the electronic contribution C_V^{el}. The experimental results, which are for C_P, are also shown. For Ni, Pd and Pt, where the Fermi level lies within (at the outer edge) the d-band, density of states $N(E_F)$ is large, resulting in a substantial contribution to C_V. In most cases the agreement with the experimental results is good, except for Ni which is ferromagnetic below the Curie temperature T_c of 627 K.[42] The discrepancy between the calculated and experimental results is largest

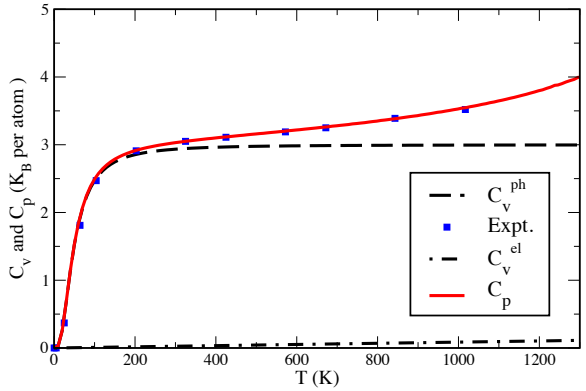

FIG. 16: Calculated temperature-dependence of heat capacity of Ag at constant volume C_V^{ph}, at constant pressure C_P and the electronic contribution C_V^{el}. The square points represent the experimental data for heat capacity at constant pressure from Ref. [63].

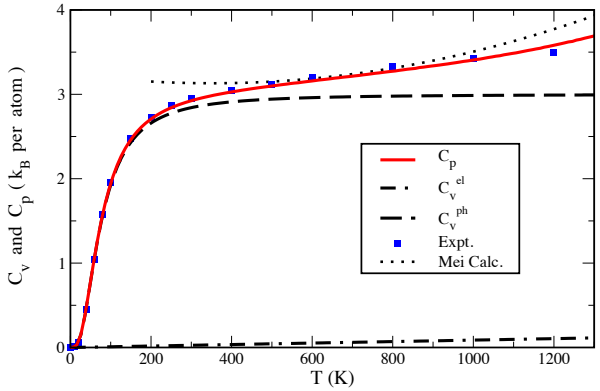

FIG. 17: Calculated temperature-dependence of heat capacity of Cu at constant volume C_V^{ph}, at constant pressure C_P and the electronic contribution C_V^{el}. The square points are the experimental data for heat capacity at constant pressure from Ref. [63]. The dotted line denotes the results from the molecular dynamics simulation of Ref. [40].

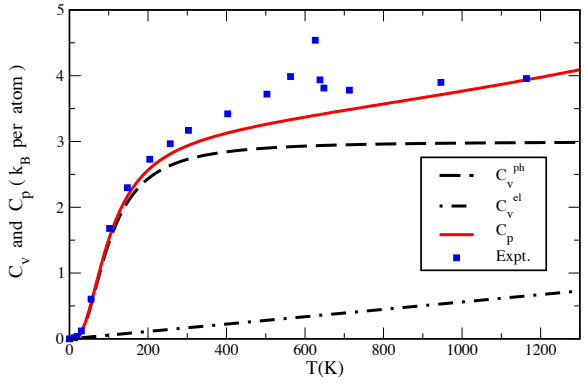

FIG. 18: Calculated temperature-dependence of heat capacity of Ni at constant volume C_V^{ph}, at constant pressure C_P and the electronic contribution C_V^{el}. The square points are the experimental data for heat capacity at constant pressure from Ref. [63].

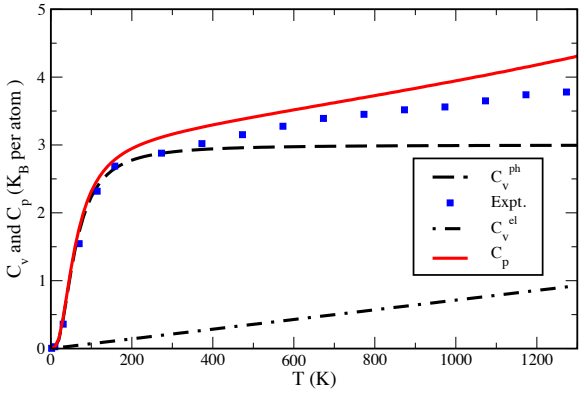

FIG. 19: Calculated temperature-dependence of heat capacity of Pd at constant volume C_V^{ph}, at constant pressure C_P and the electronic contribution C_V^{el}. The square points are the experimental data for heat capacity at constant pressure from Ref. [63].

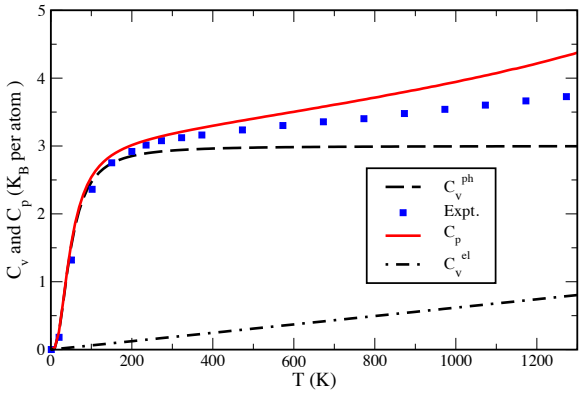

FIG. 20: Calculated temperature-dependence of heat capacity of Pt at constant volume C_V^{ph}, at constant pressure C_p and the electronic contribution C_V^{el}. The square points are the experimental data for heat capacity at constant pressure from Ref. [63].

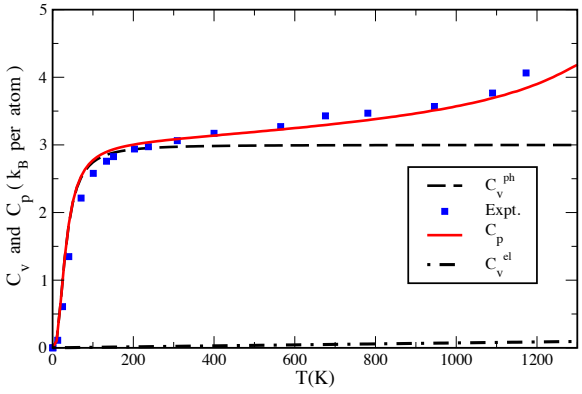

FIG. 21: Calculated temperature-dependence of heat capacity of Au at constant volume C_V^{ph}, at constant pressure C_P and the electronic contribution C_V^{el}. The square points are the experimental data for heat capacity at constant pressure from Ref. [63].

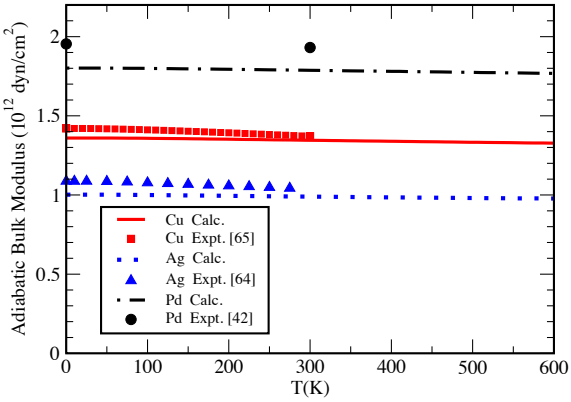

FIG. 22: Adiabatic bulk moduli $B(T)$ as a function of temperature for Ag, Cu and Pd.

at the Curie temperature and decreases steadily for temperatures both below and above T_c. For both low and high temperatures, away from T_c, the agreement is very good. The discrepancy is understandable, as the present formulation of EAM does not distinguish between the magnetic and nonmagnetic states. For Cu (Fig. (17)), the effects of anharmonicity can be seen in the dashed line, which represents the variation of C_P with temperature obtained by Mei *et al.*[40] using molecular dynamics simulation. Note that despite poor agreement between the calculated and measured phonon spectra for Au, the calculated and measured values of C_P agree very well over a large temperature range, possibly due to anharmonic effects excluded from the present calculation, which are, however, manifested in all measured properties. Poor phonon frequencies and anharmonic effects compensate for each other, yielding excellent values for C_P. Although the calculated phonon spectra for both Au and Pt show poor agreement with measured values, measured C_P for Au shows much better agreement with the calculated values than for Pt. On the contrary, measured thermal expansion is much better reproduced for Pt than for Au by the calculation.

The knowledge of C_P and C_V enables us to determine the adiabatic bulk modulus using the relation

$$B_S(T) = \frac{C_P}{C_V} B(T). \tag{22}$$

Figs.(22-23) show the calculated results. Experimental results are indicated wherever available. Both the values and the trend, a slight decrease with increasing temperature, are reproduced quite well by the model.

An important thermodynamic property is the Grüneisen parameter, which is essentially a measure of the volume-dependence of the phonon frequencies and can be related to thermal expansion[70] of the solid. The mode-specific Grüneisen Parameter corresponding to the $(\mathbf{K}, s)$ phonon mode is given by

$$\gamma_s(\mathbf{K}) = -\frac{\mathbf{V}}{\omega_{\mathbf{s}}(\mathbf{K})} \frac{\partial \omega_{\mathbf{s}}(\mathbf{K})}{\partial \mathbf{V}}. \tag{23}$$

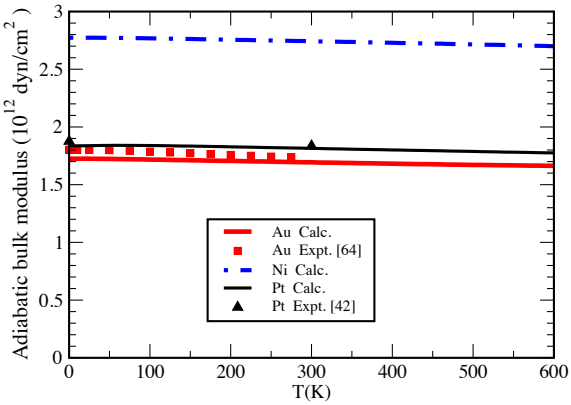

FIG. 23: Adiabatic bulk moduli $B(T)$ as a function of temperature for Au, Ni and Pt.

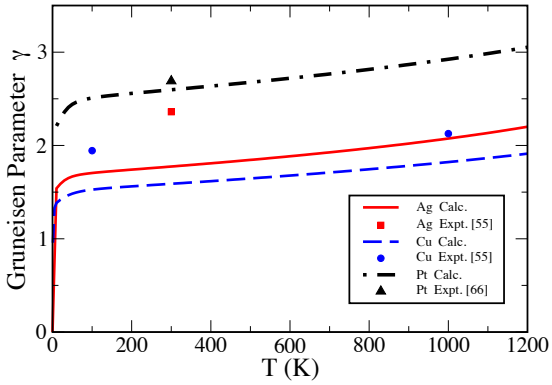

FIG. 24: Overall Grüneisen Parameter γ as a function of temperature for Ag, Cu and Pt.

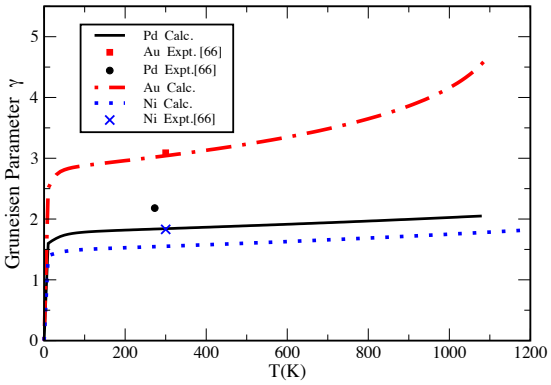

FIG. 25: Overall Grüneisen Parameter γ as a function of temperature for Au, Ni and Pd.

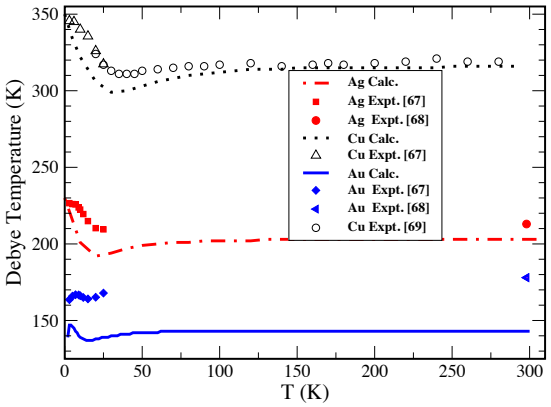

FIG. 26: Debye temperature Θ_D as a function of temperature T for Cu, Ag and Au.

We compute the overall Grüneisen parameter $\gamma(T)$ by averaging over the individual Grüneisen parameters $\gamma_s(\mathbf{K})$ of all the modes with a weight of $C_V(\mathbf{K}s)$ from each mode($\mathbf{K}s$),[70] i.e.,

$$\gamma(T) = \frac{\sum_{\mathbf{K}s} \gamma_s(\mathbf{K}) C_V(\mathbf{K}s)}{\sum_{\mathbf{K}s} C_V(\mathbf{K}s)}. \qquad (24)$$

Figs. (24 - 25) show the calculated results for the variation of the overall Grüneisen parameter $\gamma(T)$ as a function of temperature.

Finally, we study the Debye temperature and its temperature-dependence. The temperature dependent Debye temperature Θ_D is obtained by numerically evaluating the integral

$$C_V(T) = 9k_B\left(\frac{T}{\Theta_D}\right)^3 \int_0^{X_D} \frac{X^4 \exp(X)}{[\exp(X)-1]^2} dX \qquad (25)$$

with

$$X_D \equiv \Theta_D/T\,, \qquad (26)$$

and adjusting the value of X_D so that the integral on the right hand side of Eq. (25) matches the already computed value of $C_V(T)$ on the left hand side. The results are plotted in Figs.(26) and (27). The calculated values are slightly smaller than the corresponding experimental values, reflecting the difference between the calculated and the measured values of C_V. However, the maximum difference is of the order of 10%. For all metals there is an initial decrease in the Debye temperature as the temperature increases from zero, except for Au where there is an initial increase. It is interesting that the present EAM model is able to capture this trend.

V. SUMMARY OF RESULTS AND CONCLUSIONS

This work presents the first complete study of the phonon spectra and all thermodynamic properties of six fcc metals: Cu, Ag, Au, Ni, Pd and Pt, based on the EAM. The results are obtianed using the analytic embedding functions of Mei *et al.*[40] in the quasiharmonic approximation. The calculated phonon dispersion curves for Cu and Ag agree well with the inelastic neutron diffraction results. The discrepancy between the calculated and the measured phonon frequencies increases with increasing phonon wave vector for all of the above

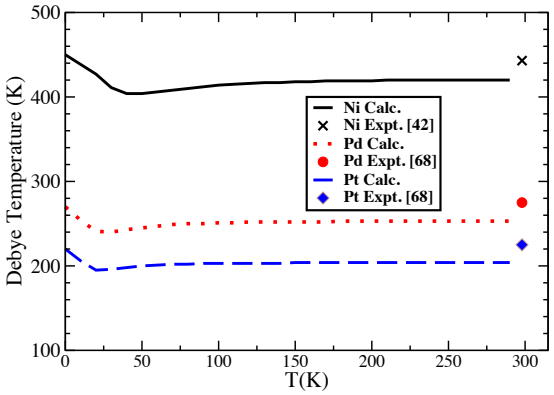

FIG. 27: Debye temperature Θ_D as a function of temperature T for Ni, Pd and Pt.

metals. However, the relative error, at the symmetry points X and L, is not more than 5.0% for Ag and 7.0% for Cu. Large differences between the calculated and the measured phonon frequencies are found for Ni, Pd, Pt and Au at high values of phonon frequencies, with the discrepancy for Au being the most drastic. However, the agreement or the lack thereof in the calculated phonon dispersion curves does not carry over to the thermodynamic properties in a proportionate way. For example, despite poor agreement for the phonon frequencies, the calculated and measured values of C_P agree very well for Au over a wide temperature range. Although the calculated phonon spectra for both Au and Pt show poor agreement with measured values, measured C_P for Au shows much better agreement with the calculated values than for Pt. On the contrary, measured thermal expansion is much better reproduced for Pt than for Au by the calculation.

Both isothermal and adiabatic bulk moduli are very well represented over a wide temperature range for all the metals studied. This is perhaps not surprising, as the parameters in the model are determined largely by fitting to the elastic constants, which usually have only very weak temperature-dependence. In general, the co-efficient of thermal expansion, calculated in the quasiharmonic approximation, is underestimated for most of the metals beyond room temperature. Calculated values of C_P for Ag, Cu and Au agree very well with the measured values. For Ni the agreement is good both below and above the Curie temperature, with the discrepancy increasing as the Curie temperature is approached from both above and below. This is understandable as the present model of EAM is not designed to capture the physics of a ferromagnetic to paramagnetic transition. The Grüneisen parameter and Debye temperature are underestimated by about 10% for all the metals. However, the temperature variation of the Debye temperature, an initial decrease as the temperature is raised from zero for all the metals except Au, is reproduced well by the model. For Au the experimental values of the Debye temperature show an initial increase. This feature is also captured by the model.

In summary, the thermodynamic properties of the six fcc metals: Cu, Ag, Au, Ni, Pd and Pt, and their temperature-dependence are reproduced reasonably well by the EAM model of Mei *et al.*.[40] The coefficient of thermal expansion is underestimated above the room tempearture in the quasiharmonic approximation used in this work. A better treatment of the anharmonicity in the potentials can improve the results, as evidenced by the molecular dynamics study of Mei *et al.*.[40] There is room for much improvement in the phonon dispersion curves for Ni, Pd, Pt and Au. There is some evidence that this can be achieved by a change in the fitting of the parameters. Preliminary calculations with small *ad hoc* changes in the parmeters representing the charge density in the model showed remarkable improvement in the phonon frequencies for Pd and Pt. This is an indication that a better representation of the charge desnity may lead to improvement for all of these metals.

ACKNOWLEDGMENTS

Financial support for this work was provided by Natural Sciences and Engineering Research Council of Canada.

* Electronic address: bianq2@univmail.cis.mcmaster.ca
† Present address: Department of Materials Science and engineering, McMaster University, Hamilton, Ontario L8S 4L8, Canada.

[1] *Interatomic Potentials and the Simulation of Lattice Defects*, edited by P.C. Gehlen, J.R. Beeler, and R.I. Jaffee (Plenum, New York, 1972).
[2] A.E. Carlsson, C.D. Gelatt Jr., and H. Ehrenreich, Phil. Mag. A **41**, 241 (1980); see also A.E. Carlsson, *Beyond Pair Potentials* in *Solid State Physics*, Volume 43, edited by Henry Ehrenreich and David Turnbull, Academic Press 1990, p.1.
[3] E. R. Cowley and R. C. Shukla, Phys. Rev. B **9**, 1261 (1974).
[4] M.W. Finnis and J.E. Sinclair, Phil. Mag. **A50**, 45 (1984).
[5] B. Legrand, Phil. Mag. B **49**, 171 (1984).
[6] V. Rosato, M. Guilope and B. Legrand, Phil. Mag. A **59**, 321 (1989), and references therein.
[7] F. Cleri and V. Rosato, Phys. Rev. B **48**, 22 (1993).
[8] Z.J. Zhang, J. Phys: Condens. Matter **10**, L495 (1998).
[9] D.G. Pettifor, J. Phys. C: Solid State Phys. **19**, 285 (1986).
[10] D.G. Pettfor, Solid State Physics, Vol. 40, edited by H. Ehrenreich and D. Turnbull (Academic Press, Inc., 1987), p. 43.
[11] F. Ducastelle and F. Cyrot-Lackmann, J. Phys. Chem. Solids **31**, 1295 (1970).
[12] F. Ducastelle and F. Cyrot-Lackmann, J. Phys. Chem. Solids **32**, 285 (1971).

[13] J. Friedel in *The Physics of Metals* (ed. J.M. Ziman), Cambridge Univ. Press, 361 (1969)
[14] R.P. Gupta, Phys. Rev. B **23**, 6265 (1981).
[15] D. Tománek, S. Mukherjee, and K.H. Bennemann, Phys. Rev. B **28**, 665 (1983).
[16] A.P. Sutton, *Electronic Structure of Materials*, Clarendon Press, Oxford, 2004, Ch. 9.
[17] D.G. Pettifor, *Bonding and Structure of Molecules and Solids*, Oxford Science Publications, 2002, Ch. 7.
[18] M.S. Daw, and M.I. Baskes, Phys. Rev. Lett. **50** 1285 (1983).
[19] M.S. Daw, and M.I. Baskes, Phys. Rev. B**29** 6443 (1984).
[20] M. Manninen, Phys. Rev. B**34** 8486 (1986).
[21] K.W. Jacobsen, J.K. Nϕrskove and M.J. Puska, Phys. Rev. B**35**, 7423 (1987).
[22] S.M. Foiles, Phys. Rev. B **32** 3409 (1985).
[23] J. Mei and J.W. Davenport , Phys. Rev. B **42** 9682 (1991).
[24] J. Mei and J.W. Davenport, Phys. Rev. B **46** 21 (1992).
[25] S.M. Foiles, M.I. Baskes and M.S. Daw, Phys. Rev. B **33** 7983 (1986).
[26] R.A. Johnson,Phys. Rev. B **39**, 12554 (1989); Phys. Rev. B **41** 9717 (1990).
[27] M.S. Daw and R.D. Hatcher, Solid State Commun. **56**, 697 (1985).
[28] J.S. Nelson, E.C.Sowa and M. S. Daw, Phys. Rev. Lett. **61** (1988).
[29] J.S. Nelson, M.S. Daw, and E.C. Sowa, Phys. Rev. B **40**, 1465 (1989).
[30] M.S. Daw and S.M. Foiles, J. Vac. Sci. Technol. A **4** 1412 (1986).
[31] S.M. Foiles, Surf. Sci. **191**, L779 (1987).
[32] T.E. Felter, S.M. Foiles, M.S. Daw and R.H. Stulen, Surf. Sci. **171** L379 (1986).
[33] M.S. Daw and S.M. Foiles, Phys. Rev. B**35** 2128 (1987).
[34] R.A. Johnson, Phys. Rev. B **37** 3924 (1988).
[35] M.S. Daw and S.M. Foiles, Phys. Rev. Lett. **59**, 2756 (1987).
[36] S.M. Foiles, Surf. Sci. **191**, 329 (1987).
[37] M.I. Baskes, Phys. Rev. B**46**, 2727 (1992).
[38] S.M. Foiles and J.B. Adams, Phys. Rev. B **40**, 5909 (1989).
[39] D.J. Oh, and R.A. Johnson, J. Mater. Res. **3**, 471 (1988).
[40] J. Mei , J.W. Davenport and G.W. Fernando, Phys. Rev. B **43**, 4653 (1991).
[41] C. Kuiying, L. Hongbo, L. Xiaoping, H. Qiyong, and H. Zhuangqi, J. Phys: Condens. Matter **7** 2379 (1995).
[42] C. Kittel, *Introduction to Solid State Physics* (John Wiley and Sons, Inc., New York, 1996).
[43] E.C. Svensson, B.N. Brockhouse and J.M. Rowe, Phys. Rev. B **155**, 619 (1967).
[44] G. Nilsson and S. Ronaldson, Phys. Rev. B **7**, 2393 (1973).
[45] E. Clementi and C. Roetti, *Atomic Data and Nuclear Tables*, Vol. 14, 177 (1974).
[46] A.D. McLean and R.S. McLean, *Atomic Data and Nuclear Tables*, Vol. 26, 197 (1981).
[47] see, for example, the full potential linear muffin-tin (FP-LMTO) results for Cu and Pd by S.Y. Savrasov and D.Y. Savrasov, Phys. Rev. B **54**, 16487 (1996).
[48] see Y. Mishin, M.J. Mehl, D.A. Papaconstantopoulos, A.F. Voter and J.D. Kress, Phys. Rev. B **63**, 224106 (2001). For the test of Cu studied by the authors, *ab initio* tight binding results for high frequency phonons are superior to those given by the two EAM schemes studied.
[49] see, for example, the pseudopotential-based results for Cu by S. Narasimhan and S. de Gironcoli, Phys. Rev. B **65**, 064302 (2002). The results are somewhat inferior to those based on the FP-LMTO method of Ref. [47] or the *ab initio* tight-binding results of Ref. [48], and also seem to depend on the scheme, LDA (local density approximation) vs. GGA (generalized gradient approximation), used to treat the exchange-correlation potential.
[50] W.A. Kamitakahara and B.N. Brockhouse, Phys. Lett. **29A**, 639 (1969).
[51] J.W. Lynn, H.G. Smith and R.M. Nicklow, Phys. Rev. B **8**, 3493 (1973).
[52] R.J. Birgeneau, J. Cordes, G. Dolling and A.D.B.woods, Phys. Rev. B **136**, A1359 (1964).
[53] A.P. Miller and B.N. Brockhouse, Can. J. Phys. **49**, 704 (1971).
[54] D.H. Dutton and B.N. Brockhouse, Can. J. Phys. **50**, 2915 (1972).
[55] R.A. MacDonald and W.M. MacDonald, Phys. Rev. B **24**, 1715 (1981).
[56] R.C. Shukla and R.A. MacDonald, High Temp.-High Press. **12**, 291 (1980).
[57] Y.S. Touloukian, R.K. Kirby, R.E. Taylor and P.D. Desai, *Thermophysical Properties of Matter, The TPRC Data Series, Thermal Expansion, Metallic Elements and alloys,* (Plenum Data Company, New York, 1977).
[58] O.K. Andersen Phys. Rev. B **8**, 3060 (1975); O.K. Andersen, O. Jepsen, and D. Glötzel, 1985, in *Highlights of Condensed Matter Theory*, edited by F. Bassani, F. Fumi, and M.P. Tosi, North-Holland, Amsterdam, 1985, pp. 59-176; O.K. Andersen, O. Jepsen, M. Sob in *Electronic structure and its applications*, edited by M. Yossouff, Lecture Notes in Physics, v.283 (Springer, Berlin,1987) p.1-57; see also http://www.fkf.mpg.de/andersen/.
[59] see for example "*Calculated electronic properties of metals*" by V.L. Moruzzi, J.F. Janak and A.R. Williams, Pergamon, New York 1978; "*Handbook of the band structure of elemental solids*" by D.A. Papaconstantopoulos, Plenum, New york, 1986.
[60] Göran Grimvall, *The Electron-phonon Interaction in Metals*, North-Holland, Amsterdam, Ch. 6 (1981).
[61] R.E. Prange and L.P. Kadanoff, Phys. Rev. **134**, A566 (1964).
[62] D.C. Wallace, *Thermodynamics of Crystals* (John Wiley and Sons, Inc., Toronto, 1972).
[63] Y.S. Touloukian and E.H. Buyco, *Thermophysical Properties of Matter, The TPRC Data Series, Specific Heat, Metallic Elements and alloys, Vol.4* (Plenum Data Company, New York, 1970).
[64] J.R. Neighbours and G.A. Alers, Phys.Rev. **111**, 707 (1958).
[65] W.C. Overton,Jr. and J. Gaffney, Phys. Rev. **98**, 969 (1955).
[66] C.V. Pandya, P.R. Vyas, T.C. Pandya and V.B. Gohel, Bull. Mater. Sci **25**, 63 (2002).
[67] D.L. Martin, Phys. Rev. **141**, 576 (1966).
[68] W.D. Compton, K.A. Gschneidner, M.T. Hutchings, H. Rabin and M.P.Tosi, *Solid States Physics, Advances in Research and Applications, Vol.16* (Academic Press, New York and London, 1964).
[69] D.L. Martin, Can. J. Phys. **38**, 2049 (1960).
[70] N.W. Ashcroft and N.D. Mermin, *Solid State Physics* (Saunders College, Philadelphia, 1976), p. 493.